

**Large ultrafast photoinduced magnetic anisotropy in a cobalt-substituted yttrium iron garnet**F. Atoneche,<sup>1</sup> A. M. Kalashnikova,<sup>1,2</sup> A. V. Kimel,<sup>1</sup> A. Stupakiewicz,<sup>3</sup> A. Maziewski,<sup>3</sup> A. Kirilyuk,<sup>1</sup> and Th. Rasing<sup>1</sup><sup>1</sup>*Radboud University Nijmegen, Institute for Molecules and Materials, Heyendaalseweg 135, 6525 AJ Nijmegen, The Netherlands*<sup>2</sup>*Ioffe Physico-Technical Institute, Russian Academy of Sciences, 194021 St. Petersburg, Russia*<sup>3</sup>*Laboratory of Magnetism, University of Bialystok, 41 Lipowa, 15-424 Bialystok, Poland*

(Received 3 February 2010; revised manuscript received 10 May 2010; published 25 June 2010)

We demonstrate experimentally that excitation of a Co-substituted ferrimagnetic yttrium iron garnet thin film with linearly polarized 100 fs laser pulses triggers large-angle magnetization precession with an amplitude, phase, and frequency determined by the characteristics of the laser pulse. The precession results from a light-induced anisotropy field with a characteristic lifetime of 20 ps, the direction of which is determined by the polarization of the light. Its strength for a pump intensity of 25 mJ/cm<sup>2</sup> is 250 G which is comparable to the intrinsic anisotropy of the sample. By choosing the proper laser-pulse parameters, we were able to excite a precession with an amplitude as large as 20° and a precession frequency modified by up to 50%.

DOI: [10.1103/PhysRevB.81.214440](https://doi.org/10.1103/PhysRevB.81.214440)

PACS number(s): 75.30.Gw, 75.78.Jp

**I. INTRODUCTION**

Traditionally, the control of the magnetization of a material is realized via the application of a magnetic field. In the pursuit to a faster speed of data manipulation, the control of the magnetization by techniques other than the application of magnetic fields has become an important area of research in recent years.<sup>1</sup> In particular, during the last decade it was demonstrated that subpicosecond light pulses can rapidly change the value of the magnetization of a medium<sup>2</sup> and/or its direction.<sup>2-4</sup> The latter implies that these laser pulses act on a magnetic medium as instantaneous effective magnetic field pulses<sup>5</sup> or modify the magnetic anisotropy,<sup>6</sup> thereby altering the magnetization direction. If the change in magnetic anisotropy is achieved via laser-induced heating,<sup>4</sup> then the subsequent slow dissipation processes considerably limit potential applications. Thus nonthermal mechanisms through which laser pulses can modify the magnetic anisotropy, resulting in a fast control of the magnetization without the heating limitation, are of particular interest.

It has recently been reported that excitation with femtosecond laser pulses leads to a nonthermal light-induced change in the magnetic anisotropy in ferrimagnetic garnets<sup>7</sup> and the ferromagnetic semiconductor GaMnAs.<sup>8</sup> Although the reported results suggested that femtosecond modulation of the magnetocrystalline anisotropy may lead to switching of the magnetization between two directions, the achieved rotation of the magnetization from its initial equilibrium position was only a fraction of a degree (0.6° and 0.8° in the garnet and GaMnAs, respectively), definitely not enough for a rotation of the magnetization over 90° or 180° required for practical applications. For that, one needs materials where photoinduced changes in the magnetocrystalline anisotropy are much stronger.

Here, we report on large-amplitude magnetization precession in a ferrimagnetic cobalt-substituted yttrium iron garnet (YIG:Co) thin film through excitation by linearly polarized 100 fs laser pulses. The deviation of the magnetization from its initial equilibrium position achieved via a photoinduced magnetic anisotropy (PMA) effect was as high as 20°. The estimated strength of the photoinduced anisotropy field is a

few hundred gauss, which is an order of magnitude larger than those previously reported.<sup>7</sup> Moreover, we observed significant changes (up to 2 GHz, that is a 50% change from the initial value) of the precession frequency as a function of light polarization, suggesting the feasibility of subpicosecond frequency modulation.

The paper is organized as follows: experimental details including sample characteristics and the experimental setup are given in Sec. II. In Sec. III we present the experimental results obtained from studies of laser-induced magnetization dynamics in YIG:Co and discuss them on the basis of a phenomenological model of PMA and the Landau-Lifshitz-Gilbert (LLG) equation.

**II. EXPERIMENTAL**

The sample under study was an 8- $\mu$ m-thick ferrimagnetic Y<sub>2</sub>CaFe<sub>4-x</sub>Co<sub>x</sub>GeO<sub>12</sub> film (YIG:Co) with a high cobalt concentration ( $x=0.08$ ), grown by liquid phase epitaxy on a (001)-oriented Gd<sub>3</sub>Ga<sub>5</sub>O<sub>12</sub> substrate (miscut about 0.1°). Its saturation magnetization at room temperature is  $4\pi M_s = 90$  G and the Néel temperature is 445 K.<sup>9,10</sup> At room temperature, the constants of uniaxial and cubic anisotropy are  $K_U = -1.1 \times 10^3$  erg/cm<sup>3</sup> and  $K_{CA} = -9.7 \times 10^3$  erg/cm<sup>3</sup>,<sup>9</sup> corresponding to anisotropy fields of about 0.15 kG and 1.36 kG, respectively, as obtained from ferromagnetic resonance (FMR) measurements. YIG:Co is known for its strong PMA effects revealed by laser excitation studies in the quasistatic regime.<sup>11,12</sup>

To study the effect of intense subpicosecond laser pulses on this photomagnetically active material, we carried out time-resolved measurements at room temperature using a magneto-optical pump-probe setup described elsewhere.<sup>4</sup> In brief, pump pulses of photon energy 1.55 eV with a duration of 100 fs and a repetition rate of 500 Hz were directed at an angle of incidence of 10° from the sample normal parallel to the [001] crystallographic axis while the probe pulses with the same energy of 1.55 eV were incident along the sample normal, see Fig. 1. The pump beam was focused to a spot of about 250  $\mu$ m in diameter and the probe spot was about two times smaller. The probe to pump intensity ratio was about

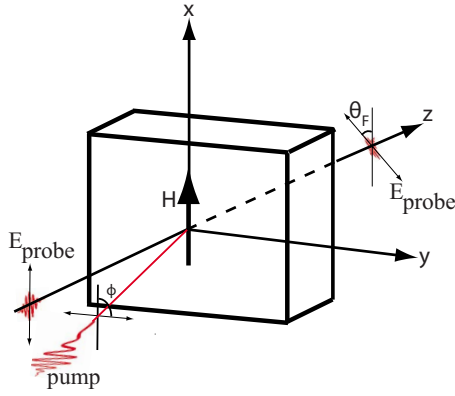


FIG. 1. (Color online) Sample orientation and experimental geometry with magnetic field applied along the [100] axis.  $x$ ,  $y$ , and  $z$  are parallel to the [100], [010], and [001] directions, respectively.

1:100. The delay time  $\Delta t$  between the pump and the probe pulses could be adjusted up to 3 ns with a resolution down to 10 fs. The angle  $\phi$  between the plane of polarization of the pump pulses and the [100] axis could be varied, see Fig. 1. The Faraday rotation angle  $\theta_F$  of the probe pulses as a function of the delay time  $\Delta t$  was measured. In this configuration, the transient Faraday rotation  $\theta_F(\Delta t)$  is proportional to the dynamical out-of-plane component  $M_z(\Delta t)$  of the magnetization. An external magnetic field was applied either along the [100] ( $H_{ext}=H_{100}$ ) or [110] ( $H_{ext}=H_{110}$ ) direction.

III. RESULTS AND DISCUSSION

Figure 2 shows the transient Faraday rotation  $\theta_F$  of the probe polarization as a function of the delay time  $\Delta t$  for different values of the applied magnetic field  $H_{100}$ . Pronounced oscillations are observed with an amplitude and frequency dependent on the applied field. Examination of the

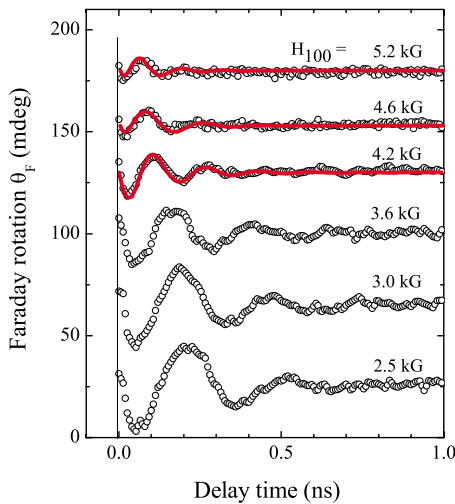


FIG. 2. (Color online) Faraday rotation  $\theta_F$  of the probe beam as a function of the delay time between pump and probe pulses for different values of the applied magnetic field  $H_{100}$ . Lines are simulations (see text). All results were obtained for  $\phi=90^\circ$  and a pump intensity of 25 mJ/cm<sup>2</sup>.

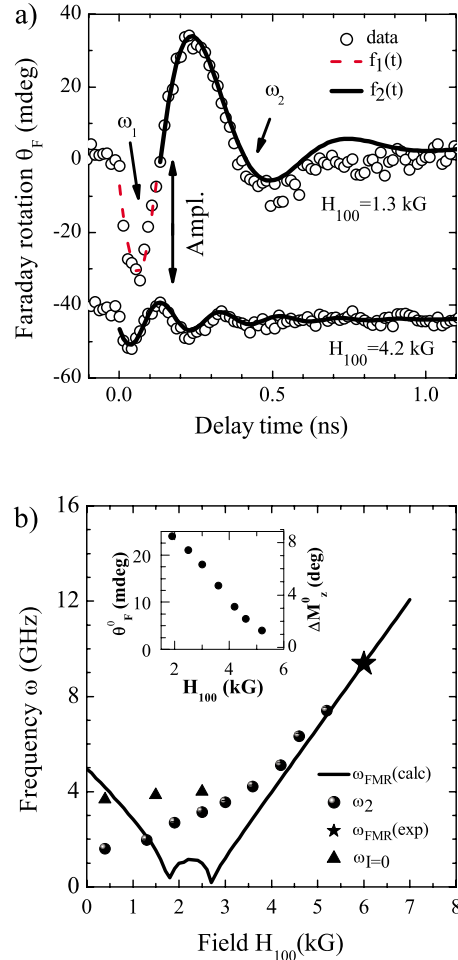


FIG. 3. (Color online) (a) Representative curves  $\theta_F(\Delta t)$  for 1.3 and 4.2 kG and their fits to the functions  $f_1$  (dashed line) and  $f_2$  (solid line) as described in the text. (b) Frequency  $\omega_2$  as a function of the external field  $H_{100}$ . Also shown is the calculated FMR frequency curve for our geometry (line) and the measured  $\omega_{FMR}$  (star) (Ref. 16). Triangles show the frequency  $\omega_{I=0}=\omega_2(I=0$  mJ/cm<sup>2</sup>) obtained from  $\omega(I)$  curves by extrapolation to  $I=0$  mJ/cm<sup>2</sup> (see Fig. 6). The inset of (b) shows the precession amplitude  $\theta_F^0$  with the corresponding deviation angle  $\Delta M_z^0$  vs applied field  $H_{100}$ .

observed oscillations shows that, at low fields ( $<2.5$  kG), they are not characterized by a single frequency [see the top curve in Fig. 3(a)]. Therefore, we fitted the curves obtained for low fields with two sinusoidal functions. For the delay-time interval 0–150 ps, the function  $f_1(\Delta t)=A_1 \sin(\omega_1 \Delta t + \psi_1)$  was used; for delay times longer than 150 ps, the function  $f_2(\Delta t)=A_2 \exp(-\Delta t/\tau) \sin(\omega_2 \Delta t + \psi_2)$ . The curves for fields larger than 2.5 kG were fitted with the single function  $f_2(\Delta t)$ . Figure 3(b) shows that the frequency  $\omega_2$  increases with increasing applied field and for  $H_{100}>3$  kG corresponds to the FMR frequency  $\omega_{FMR}$  of the sample. The frequency  $\omega_1=3$  GHz is independent of the applied field  $H_{100}$ . The presence of the two time scales ( $1/\omega_1$  and  $1/\omega_2$ ) at low applied fields indicates that the magnetization precesses in an effective field which changes with time after laser excitation. Remarkably, the magnetization deviation angle (of up to  $10^\circ$ ) derived from the precession amplitude, exceeds those re-

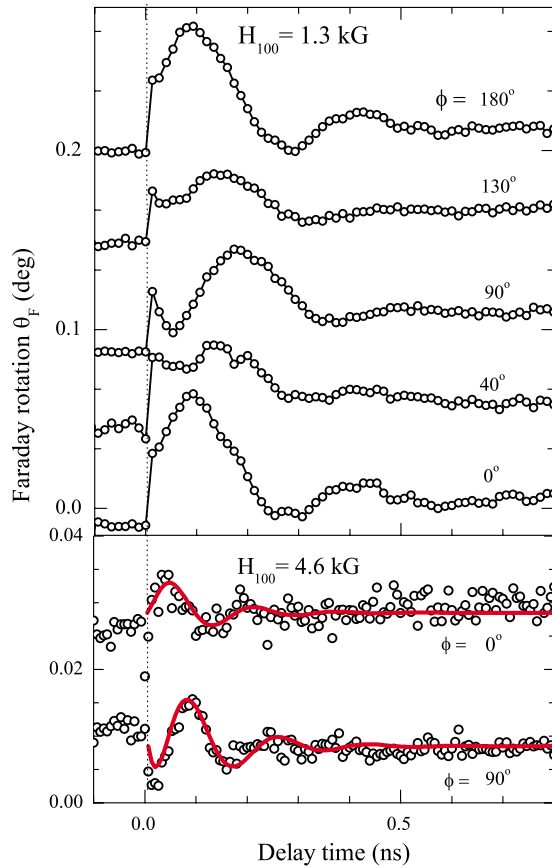


FIG. 4. (Color online) Rotation of the plane of polarization of the probe as a function of the delay time between pump and probe pulses measured for different planes of polarization of the pump  $\phi$  for an applied field of 1.3 kG (upper panel) and 4.6 kG (lower panel). The pump intensity was 25 mJ/cm<sup>2</sup>. The solid lines indicate simulated curves.

ported earlier by more than an order of magnitude [see the inset of Fig. 3(b)].

To understand the origin of the light-induced precession, we studied its dependence on the pump polarization  $\phi$ . Figure 4 shows the transient Faraday rotation  $\theta_F$  of the probe polarization as a function of the delay time  $\Delta t$  for different planes of polarization of the pump  $\phi$  for representative applied fields of 1.3 kG (upper panel) and 4.6 kG (lower panel). The precession changes noticeably as the angle  $\phi$  is gradually varied. In the upper panel of Fig. 5, the precession amplitude is plotted as a function of  $\phi$  for a field  $H = 0.4$  kG applied along the [100] and [110] crystallographic axes. A clear periodic dependence of the precession amplitude on the polarization angle is observed, which is independent of the applied field direction. The amplitude of the precession is maximum but with a different initial phase, for pulses polarized either along or perpendicular to the [100] axis. We note that minimization of the total magnetic energy gives a difference of  $\approx 6^\circ$  between the  $xy$  projections of the equilibrium magnetization orientation for the applied fields  $H_{100}=H_{110}=0.4$  kG. This difference increases to  $45^\circ$  at  $H_{100}=H_{110}=2.5$  kG. Therefore, the fact that the maximum always occurs at the same angle  $\phi$  irrespective of the applied field orientation and strength shows that the observed effect

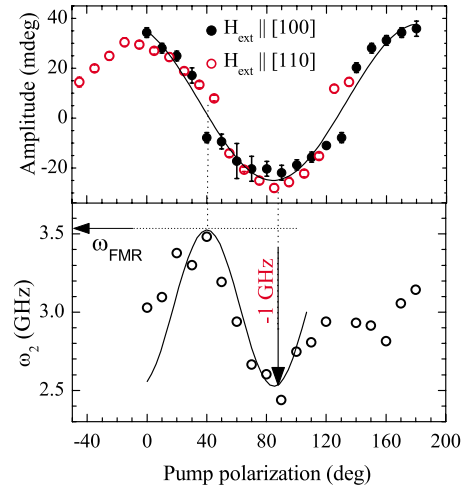


FIG. 5. (Color online) Precession amplitude (upper panel) and precession frequency  $\omega_2$  (lower panel) as a function of  $\phi$ .

depends on the orientation of the light polarization plane with respect to the crystallographic axes only. This dependence on polarization allows us to conclude that the photoinduced effect is of nonthermal origin.

The observed polarization dependence (Figs. 4 and 5) and the fact that the effective field is time dependent suggest that the microscopic origin of the observed process is a PMA change. In general, for magnetic garnets, the dependence of the photoinduced effects on the polarization of light reflects the symmetry of the site that hosts the anisotropic photoactive centers.<sup>13</sup> Up to 0.5 Co<sup>2+</sup> and 2 Co<sup>3+</sup> ions per formula unit can substitute Fe<sup>3+</sup> ions. Co<sup>2+</sup> and Co<sup>3+</sup> ions that occupy octahedral sites and tetrahedral sites contribute differently to the PMA for a fixed polarization plane. In our experiments, the maximum effect induced by linearly polarized 100 fs laser pulses occurs for  $\phi=0^\circ$  and for  $\phi=90^\circ$ . That is, when light is polarized parallel to the [100] or [010] crystallographic axes [see Fig. 1(a)], which are also the local symmetry axes of the tetrahedral sites in YIG:Co. For light polarized along the [110] direction ( $\phi=45^\circ$ ), which is also an in-plane symmetry direction with respect to the tetrahedral sites (i.e., a global symmetry axis), the orientational distribution of the photomagnetic centers remains the same.<sup>13</sup> Therefore, the symmetry of the magnetic properties (in particular, the symmetry of the local anisotropy contribution from photoexcited Co ions in tetrahedral positions) is unchanged, resulting in a minimum of the magnetization precession when  $\phi=45^\circ$  (see Figs. 4 and 5). Thus, the polarization-dependent excitation of the precession can be attributed to a change in the magnetic anisotropy due to the laser-induced modification of the local anisotropy contribution from Co ions in tetrahedral positions. We note that this is in contrast to the quasistatic photomagnetic anisotropy observed in YIG:Co films subjected to 488 nm radiation,<sup>11</sup> which was related to charge transfer between Co ions occupying octahedral crystallographic positions. This difference can easily be understood: for the excitation light wavelength in the near IR range used in our experiments, absorption is mainly due to ions in the noncentrosymmetric tetrahedral positions<sup>14,15</sup> and, therefore, the photomagnetic effect is expected to be domi-

nated by the contribution of Co ions in these sites. Moreover, the previously reported photoinduced magnetic anisotropy due to the octahedral coordinated Co ions possessed a very long relaxation time (up to 100 s) and, thus, is not accessible by stroboscopic-type pump-probe experiments with a repetition rate of 500 Hz as in our experiments.

**Landau-Lifshitz-Gilbert equation model including PMA**

To further investigate the excitation of the magnetization precession due to the PMA effect and to obtain the parameters of the photoinduced change in the anisotropy, we performed macrospin simulations of the magnetization precession using the LLG,

$$\frac{d\mathbf{M}}{dt} = \frac{\gamma}{1 + \alpha^2} \left[ [\mathbf{M} \times \mathbf{H}_{\text{eff}}(t)] + \frac{\alpha}{M} \{ \mathbf{M} \times [\mathbf{M} \times \mathbf{H}_{\text{eff}}(t)] \} \right], \quad (1)$$

where a time-varying effective magnetic field  $\mathbf{H}_{\text{eff}}(t)$  is introduced to describe the light-induced modification of the magnetic anisotropy.  $\gamma = 17.6 \times 10^6 \text{ Oe}^{-1}$ , is the gyromagnetic ratio and  $\alpha$  is the phenomenological Gilbert damping parameter. The damping parameter used in the simulation was  $\alpha = 0.25$  which is in agreement with  $\alpha = 0.23$  obtained from room-temperature FMR measurements for this sample.<sup>16</sup> The coordinate system is such that the sample lies in the  $x$ - $y$  plane, with the sample crystallographic axes  $[100]$ ,  $[010]$ , and  $[001]$  parallel to the Cartesian  $x$ ,  $y$ , and  $z$  axes, respectively, as shown in Fig. 1(a). Initially, the equilibrium direction of the magnetization  $\mathbf{M}$  in a uniformly magnetized magnetic material is along the effective field  $\mathbf{H}_{\text{eff}}(\Delta t < 0)$ , given by

$$\mathbf{H}_{\text{eff}}(\Delta t < 0) = \mathbf{H}_{\text{ext}} + \mathbf{H}_A + \mathbf{H}_D. \quad (2)$$

In our model,  $\mathbf{H}_{\text{ext}} = (\mathbf{H}_x, 0, 0)$  is the applied magnetic field and  $\mathbf{H}_D = -4\pi(\mathbf{M}_x, \mathbf{M}_y, \mathbf{M}_z)$  is the demagnetizing field.  $\mathbf{H}_A = \mathbf{H}_{CA} + \mathbf{H}_U$  is the sum of all internal (cubic and uniaxial) anisotropy fields. The cubic magnetocrystalline anisotropy field

$$\mathbf{H}_{CA} = -\nabla_{\mathbf{M}} E_{CA}. \quad (3)$$

In Eq. (3),  $E_{CA}$  is the standard expression for the cubic anisotropy energy in Cartesian coordinates, neglecting terms of order higher than 4. The uniaxial anisotropy field is entered as  $\mathbf{H}_U = (0, 0, \mathbf{H}_U)$ .

The photoinduced modification of the magnetic anisotropy is modeled as an appearance of an additional time-dependent term  $\mathbf{H}_L(t)$  in the expression of  $\mathbf{H}_{\text{eff}}$ .  $\mathbf{H}_L(t)$  is an exponentially decaying anisotropy field

$$\mathbf{H}_L(t < 0) = 0, \quad \mathbf{H}_L(t > 0) = \mathbf{H}_L^{\text{max}}(e^{-t/\tau}) \quad (4)$$

with a rise time assumed to be within 100 fs and approximated as a step function, and a decay time  $\tau$ . The light modified effective field is then given by

$$\mathbf{H}_{\text{eff}}(\Delta t > 0) = \mathbf{H}_{\text{ext}} + \mathbf{H}_A + \mathbf{H}_D + \mathbf{H}_L(t). \quad (5)$$

At each time step in the simulation, the fields are recalculated from the values of the magnetization obtained from the preceding time.

Figure 1(b) (solid lines) shows the results of the simulations of the magnetization dynamics based on Eqs. (1)–(5) for different applied field values. Good agreement between experimental and simulated curves is obtained for the following parameters:  $H_L^{\text{max}} = 0.25 \text{ kG}$  and  $\tau = 20 \text{ ps}$ . A lifetime between 10 and 20 ps (with a corresponding renormalization of the amplitude between 0.25 and 0.4 kG) may also be used to fit the experimental data because  $\tau = 20 \text{ ps}$  is short compared to the precession period. These results show that the optically induced anisotropy is of the same order of magnitude as the intrinsic fields. We note that the light-induced anisotropy field strength obtained here is an order of magnitude larger than those reported earlier.<sup>6,8</sup>

The directions of the light-induced anisotropy field  $\mathbf{H}_L$  found from the simulations are as follows: when the polarization is parallel or perpendicular to the applied field direction (i.e.,  $[100]$  axis), the light-induced anisotropy field  $\mathbf{H}_L$  is along the  $[101]$  or  $[011]$  direction, respectively, independent of the intensity. The lower panel of Fig. 4 shows the results of simulations (solid lines) for the two light-induced anisotropy field directions for an applied field of 4.6 kG. Good agreement between measured and simulated curves is achieved, showing that the polarization plane of the light defines the direction of the light-induced anisotropy while the light intensity determines its strength.

The experimental data and the simulations described above agree well in the range of high applied fields. As the applied field  $H_{100}$  decreases, noticeable deviations between simulations and experiments appear. First, in the low magnetic field range, the magnetization precession frequency deviates from the FMR frequency and changes from  $\omega_1$  to  $\omega_2$  during the precession [see Fig. 3(a)]. Second, the frequency during the first 150 ps,  $\omega_1 = 3 \text{ GHz}$ , is independent of the applied field, within the precision of the fit. For applied fields below 1 kG, the precession frequency  $\omega_2$  appears to be smaller than  $\omega_{\text{FMR}}$  [Fig. 3(b)], with the difference becoming stronger as the applied field reduces. A similar behavior was observed for  $H_{110}$ .

However, the proposed model of the light-induced anisotropy provides an understanding of the precession excitation process even at low fields. Right after the laser pulse the magnetic moments start to precess around the new effective field given by Eq. (5), which decays to its equilibrium value with a characteristic time of  $\tau = 20 \text{ ps}$ . Therefore, for low applied fields, the precession frequency during  $3\tau$  is mostly defined by the internal and light-induced anisotropy fields, which explains the appearance of the field-independent frequency  $\omega_1$ . After this time the precession frequency of the magnetization can be expected to be equal to the ferrimagnetic resonance frequency  $\omega_{\text{FMR}}$ . This is, however, not the case: for  $H_{100} < 1 \text{ kG}$ , the frequency  $\omega_2$  is lower than  $\omega_{\text{FMR}}$ , as can be seen from Fig. 3(b). A closer look at the precession at low fields excited by light with different polarizations, shows that  $\omega_2$  varies as a function of  $\phi$  (Fig. 5, lower panel) and the minimum and maximum values of  $\omega_2$  occur for pump polarizations  $\phi = 0, 90^\circ$ , and  $\phi = 45^\circ$ , respectively, pointing to a correlation between this polarization dependence and the previously discussed precession amplitude dependence on polarization (see Fig. 5, upper panel). Note that  $\omega_2$  approaches  $\omega_{\text{FMR}}$  when  $\phi = 45^\circ$ , i.e., when the PMA effect

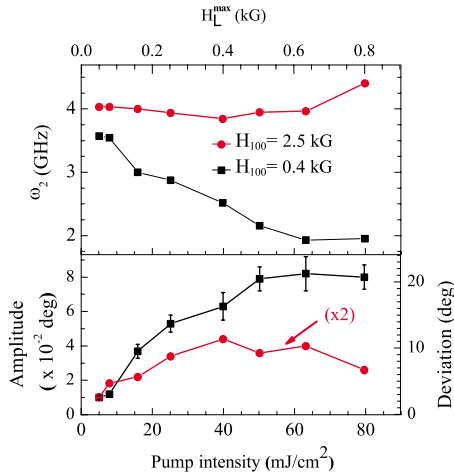


FIG. 6. (Color online) Precession frequency  $\omega_2$  (upper panel) as a function of pump intensity for applied field values of (i) 0.4 kG (squares) and (ii) 2.5 kG (spheres). Error bars are smaller than the data point markers. The top axis shows the photoinduced field  $H_L^{\max}$ , corresponding to the intensity of the bottom axis. Precession amplitude (lower panel) as a function of pump intensity for applied field values of (i) 0.4 kG (squares) and (ii) 2.5 kG (spheres). The corresponding estimated deviation angles of the magnetization from equilibrium are plotted on the right  $Y$  axis. The results are obtained for  $\phi=90^\circ$ .

is minimal. To further investigate the light-induced nature of the effect we studied the dependence of the amplitude and frequency on pump pulse intensity. The upper panel of Fig. 6 shows the dependence of  $\omega_2$  on intensity for two values of the applied field. For a field of 0.4 kG, a decrease in frequency with increasing pump intensity is observed, accompanied simultaneously by an increase in amplitude (lower panel). Again  $\omega_2$  approaches  $\omega_{\text{FMR}}$  as the pump intensity approaches zero, i.e., when the light-induced contribution is minimal. As the applied field increases, the frequency dependence on pump intensity becomes less pronounced and disappears at fields larger than  $\sim 2.5$  kG while the amplitude dependence on intensity remains qualitatively the same. This dependence of the precession amplitude and frequency on pump polarization and pump intensity suggests that the observed change in  $\omega_2$  is photoinduced and is related to the optical excitation of the magnetization precession. Note that this observation demonstrates the feasibility of modulation of the FMR frequency with the help of subpicosecond laser pulses.

One might argue that light-induced heating can lead to changes in the magnetocrystalline anisotropy constants and, consequently, resulting in the observed frequency variations. In a dichroic material, this effect is indeed dependent on polarization. However, for the pump fluences used in the experiments (below 80 mJ/cm<sup>2</sup>), the estimated<sup>17</sup> light-induced increase in the temperature is below 10 K, which cannot account for the observed variation in the FMR frequency, given that no spin-reorientation phase transitions were observed in the vicinity of room temperature.<sup>9,18</sup> Moreover, no significant optical dichroism was reported for iron garnets in the optical range relevant for our measurements. For polarization-dependent heating, for example, resulting

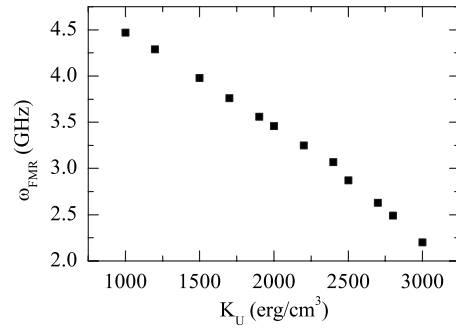


FIG. 7. Ferromagnetic resonance frequency  $\omega_{\text{FMR}}$  as a function of the uniaxial anisotropy constant  $K_U$  calculated from the FMR formula (Ref. 20). The external field was constant at 0.4 kG applied along the [100] crystallographic direction.

from dichroism, the expected polarization dependence period is  $180^\circ$ , i.e., a minimum and maximum precession amplitude at  $0^\circ$  and  $90^\circ$ , respectively. This is in contrast to our observed minimum and maximum precession at  $45^\circ$  and  $0^\circ$ , respectively. Thus, polarization-dependent heating cannot be the underlying mechanism for the excitation of magnetization precession and the change in frequency.

Although the observed dependence of the effect on light polarization, described by the introduction of  $\mathbf{H}_L$  in the model above, suggests an involvement of tetrahedrally coordinated cobalt ions in the process,  $\mathbf{H}_L$  alone does not explain the frequency deviation from  $\omega_{\text{FMR}}$  observed at low fields. However, tetrahedrally coordinated cobalt is known to be responsible for the growth-induced anisotropy in YIG:Co.<sup>19</sup> Therefore, a light-induced excitation of these cobalt sites may lead to a change in the uniaxial anisotropy. To understand the influence of a change in the uniaxial anisotropy on the FMR frequency, we performed a simple analysis of the dependence of the FMR frequency on the strength of the former, based on the Kittel formula.<sup>20</sup> Figure 7 shows the dependence of the frequency  $\omega_{\text{FMR}}$  on the uniaxial anisotropy constant for an applied field of 0.4 kG. This analysis at a low applied field shows that a change in the uniaxial anisotropy constant  $K_U$  by a factor of 2 leads to noticeable changes in the FMR frequency. On the contrary, at high fields (not shown), there is no significant frequency change. Therefore the analysis correctly describes our experimental observations. We note that in the soft-mode range,  $1 < H_{100} < 3$  kG, the precession frequency exceeds the calculated FMR frequency, which appears to be a common feature observed in light-induced precession<sup>21,22</sup> and is likely related to the inhomogeneous profile of the excitation light pulse.

The experimental observations and model presented above therefore allow us to conclude that femtosecond optical excitation of YIG:Co gives rise to a strong nonthermal PMA, which is most noticeable at low applied fields. For example, at 0.4 kG, we obtained a deviation angle for the magnetization of  $20^\circ$  at a pump intensity of 60 mJ/cm<sup>2</sup> (see the lower panel of Fig. 6). This deviation angle exceeds significantly any others reported for nonthermal light-induced magnetization precession so far. A further increase in intensity did not lead to any increase in the deviation angle due to saturation, when all cobalt ions present are involved in ab-

sorption. We note that no optically induced sample damage was observed in the range of intensities used in our experiments. However, white light generation from the sample is observed at pump intensities just over  $70 \text{ mJ/cm}^2$ , indicating the upper limit of suitable intensities. With the role of cobalt identified, achieving even larger deviation angles and subsequent magnetization reversal will require samples with a tetrahedral site cobalt concentration higher than the present.

#### IV. CONCLUSIONS

In conclusion, we observed magnetization precession in a ferrimagnetic YIG:Co thin film due to the appearance of a light-induced anisotropy after excitation with 100 fs linearly polarized laser pulses. The strength of the photoinduced anisotropy field is of the order of a few hundred gauss, which is comparable to the intrinsic anisotropy of the sample but exceeds by an order of magnitude those reported earlier. The magnetization deviation angle from equilibrium achieved is

as high as  $20^\circ$ . Moreover, we also observe significant precession frequency variations resulting from a light-induced modification of the cobalt-mediated growth-induced magnetic uniaxial anisotropy. This significant photoinduced change in the magnetic-resonance frequency observed shows the feasibility of modulation of the frequency of FMR at time scales much shorter than the period of spin precession.

#### ACKNOWLEDGMENTS

We thank B. A. Ivanov and R. V. Pisarev for insightful discussions, A. J. Toonen and A. van Etteger for technical assistance, and R. Gieniusz for FMR measurements. This work was supported by the Dutch nanotechnology initiative NanoNed, de Nederlandse Organisatie voor Wetenschappelijk Onderzoek (NWO), Stichting voor Fundamenteel Onderzoek der Materie (FOM), Russian Foundation for Basic Research under Grant No. 10-02-01008-a, and the EU Seventh Framework Programme (FP7/2007-2013) under grant Agreements No. NMP3-SL-2008-214469 (UltraMag-netron) and No. N 214810 (FANTOMAS).

- 
- <sup>1</sup>J. Stöhr and H. C. Siegmann, *Magnetism: From Fundamentals to Nanoscale Dynamics* (Springer-Verlag, Berlin, 2006).
- <sup>2</sup>E. Beaurepaire, J. C. Merle, A. Daunois, and J. Y. Bigot, *Phys. Rev. Lett.* **76**, 4250 (1996).
- <sup>3</sup>C. D. Stanciu, F. Hansteen, A. V. Kimel, A. Kirilyuk, A. Tsukamoto, A. Itoh, and Th. Rasing, *Phys. Rev. Lett.* **99**, 047601 (2007).
- <sup>4</sup>A. V. Kimel, A. Kirilyuk, A. Tsvetkov, R. V. Pisarev, and Th. Rasing, *Nature (London)* **429**, 850 (2004).
- <sup>5</sup>A. V. Kimel, A. Kirilyuk, P. A. Usachev, R. V. Pisarev, A. M. Balbashov, and Th. Rasing, *Nature (London)* **435**, 655 (2005).
- <sup>6</sup>F. Hansteen, A. V. Kimel, A. Kirilyuk, and Th. Rasing, *Phys. Rev. B* **73**, 014421 (2006).
- <sup>7</sup>F. Hansteen, A. V. Kimel, A. Kirilyuk, and Th. Rasing, *Phys. Rev. Lett.* **95**, 047402 (2005).
- <sup>8</sup>Y. Hashimoto, S. Kobayashi, and H. Munekata, *Phys. Rev. Lett.* **100**, 067202 (2008).
- <sup>9</sup>M. Tekielak, A. Stupakiewicz, A. Maziewski, and J. M. Desvignes, *J. Magn. Magn. Mater.* **254-255**, 562 (2003).
- <sup>10</sup>A. Maziewski, *J. Magn. Magn. Mater.* **88**, 325 (1990).
- <sup>11</sup>A. Stupakiewicz, A. Maziewski, I. Davidenko, and V. Zablotskii, *Phys. Rev. B* **64**, 064405 (2001).
- <sup>12</sup>A. B. Chizhik, I. I. Davidenko, A. Maziewski, and A. Stupakiewicz, *Phys. Rev. B* **57**, 14366 (1998).
- <sup>13</sup>A. Tucciarone, in *Physics of Magnetic Garnets*, Proceedings of the International School of Physics "Enrico Fermi," Course LXX, edited by A. Paoletti (North-Holland, Amsterdam, 1978).
- <sup>14</sup>B. Antonini, M. Marinelli, E. Milani, A. Paoletti, P. Paroli, J. Daval, and B. Ferrand, *Phys. Rev. B* **39**, 13442 (1989).
- <sup>15</sup>We note that the observed effect does possess any resonant behavior (for pump photon energies between 1.54 and 2.15 eV) and therefore, cannot be associated with a particular optical transition.
- <sup>16</sup>A. Stupakiewicz (private communication).
- <sup>17</sup>In order to estimate the temperature increase, we used the heat capacity  $C=900 \text{ J/(mol K)}$  [P. Novak, in *Numerical Data and Functional Relationships in Science and Technology*, Landoldt-Börnstein, New Series, Group III Vol. 27, Pt. E (Springer-Verlag, Berlin, 1970)]; and an absorption coefficient of  $\alpha = 100 \text{ cm}^{-1}$  [D. L. Huber, in *Numerical Data and Functional Relationships in Science and Technology*, Landoldt-Börnstein, New Series, Group III Vol. 4, Pt. A (Springer-Verlag, Berlin, 1970)].
- <sup>18</sup>M. Tekielak, Ph.D. thesis, University of Bialystok, 1997.
- <sup>19</sup>E. M. Gyorgy, L. C. Luther, R. C. LeCraw, and S. L. Blank, *J. Appl. Phys.* **52**, 2326 (1981).
- <sup>20</sup>J. O. Artman, *Phys. Rev.* **105**, 74 (1957).
- <sup>21</sup>A. V. Kimel, C. D. Stanciu, P. A. Usachev, R. V. Pisarev, V. N. Gridnev, A. Kirilyuk, and Th. Rasing, *Phys. Rev. B* **74**, 060403 (2006).
- <sup>22</sup>C. D. Stanciu, A. V. Kimel, F. Hansteen, A. Tsukamoto, A. Itoh, A. Kirilyuk, and Th. Rasing, *Phys. Rev. B* **73**, 220402(R) (2006).